Geophys. J. Int. (2006) **167,** 223–237 doi: 10.1111/j.1365-246X.2006.03044.x

Analysis of the crustal velocity structure of the British Isles using teleseismic receiver functions

J. P. Tomlinson,[1,2,*] P. Denton,[1] P. K. H. Maguire[1] and D. C. Booth[2]

[1]*Department of Geology, University of Leicester, University Road, Leicester,* LE1 7RH, *UK. E-mail: james.tomlinson@ohmsurveys.com*
[2]*British Geological Survey, Murchison House, West Mains Road, Edinburgh,* EH9 3LA, *UK*

Accepted 2006 April 20. Received 2006 March 7; in original form 2004 December 16

SUMMARY

The onshore crustal and upper mantle velocity structure of the British Isles has been investigated by teleseismic receiver function analysis. The results of the study augment the dense offshore and sparse onshore models of the velocity structure beneath the area. In total almost 1500 receiver functions have been analysed, which have been calculated using teleseismic data from 34 broadband and short-period, three-component seismic recording instruments. The crustal structure has primarily been investigated using 1-D grid search and forward modelling techniques, returning crustal thicknesses, bulk crustal V_p/V_s ratio and velocity-depth models. $H - \kappa$ stacking reveals crustal thicknesses between 25 and 36 km and V_p/V_s ratios between 1.6 and 1.9. The crustal thicknesses correlate with the results of previous seismic reflection and refraction profiles to within ± 2 km. The significant exceptions are the stations close to the Iapetus Suture where the receiver function crustal thicknesses are up to 5 km less than the seismic refraction Moho. This mismatch could be linked to the presence of underplated magmatic material at the base of the crust. 1-D forward modelling has revealed subcrustal structures in northern Scotland. These correlate with results from other UK receiver function studies, and correspond with the Flannan and W-reflectors. The structures are truncated or pinch out before they reach the Midland Valley of Scotland. The isolated subcrustal structure at station GIM on the Isle of Man may be related to the closure of the Iapetus Ocean.

Key words: British Isles, crust, Moho discontinuity, receiver functions.

1 INTRODUCTION

The dominating structure within the crust of the British Isles is the Iapetus Suture. This northeast–southwest trending feature represents the boundary between Laurentian crust to the north, and Avalonian crust to the south, and was formed during the closure of Iapetus some 380 Ma. The oblique motion of the closure brought together a number of terranes on the southern margin of Laurentia, with which Avalonia subsequently collided (Fig. 1). Since the Caledonian Orogeny the British Isles have been characterized by the erosion of uplifted blocks and the deposition of the resultant sediments into basins, with this architecture being controlled by episodes of both compression and extension. The most significant of these events was the Variscan Orogeny. This was followed by Jurassic seafloor spreading in the central Atlantic, which initiated North Sea graben formation, and Cretaceous rifting in the North Atlantic and North Sea. The formation of Iceland on the mid-Atlantic ocean ridge has been associated with Cenozoic uplift and denudation in the British Isles. It has been suggested that permanent uplift (as opposed to temporary, dynamic uplift) has been caused by low-density magma sourced directly from the upwelling Iceland Plume underplating parts of the crust of the British Isles (Jones *et al.* 2002), with the maximum denudation (and therefore, the maximum amount of underplate) occurring in the East Irish Sea, northern England region.

The juxtaposed Laurentian and Avalonian structures of the British Isles have been the target of a large number of geophysical studies. The British Institutions Reflection Profiling Syndicate (BIRPS) carried out surveys along a number of offshore profiles (Klemperer & Hobbs 1991) typically identifying a two layer crust, with a transparent upper crust overlying a highly reflective lower crust (McGeary *et al.* 1987). The profiles along the east and west coasts of the British Isles show a group of north-dipping crustal reflectors which strike parallel to the dominant Caledonian trend. These have been identified as the subsurface expression of the Iapetus Suture (Freeman *et al.* 1988; Brewer *et al.* 1983). The Lithospheric Seismic Profile in Britain (LISPB) (Bamford *et al.* 1978) and the Caledonian Suture Seismic Experiment (CSSP) (Bott *et al.* 1985; Al-Kindi *et al.* 2003) are two deep seismic wide-angle reflection/refraction

*Now at: Offshore Hydrocarbon Mapping, Technology Centre, Claymore Drive, Aberdeen, UK.

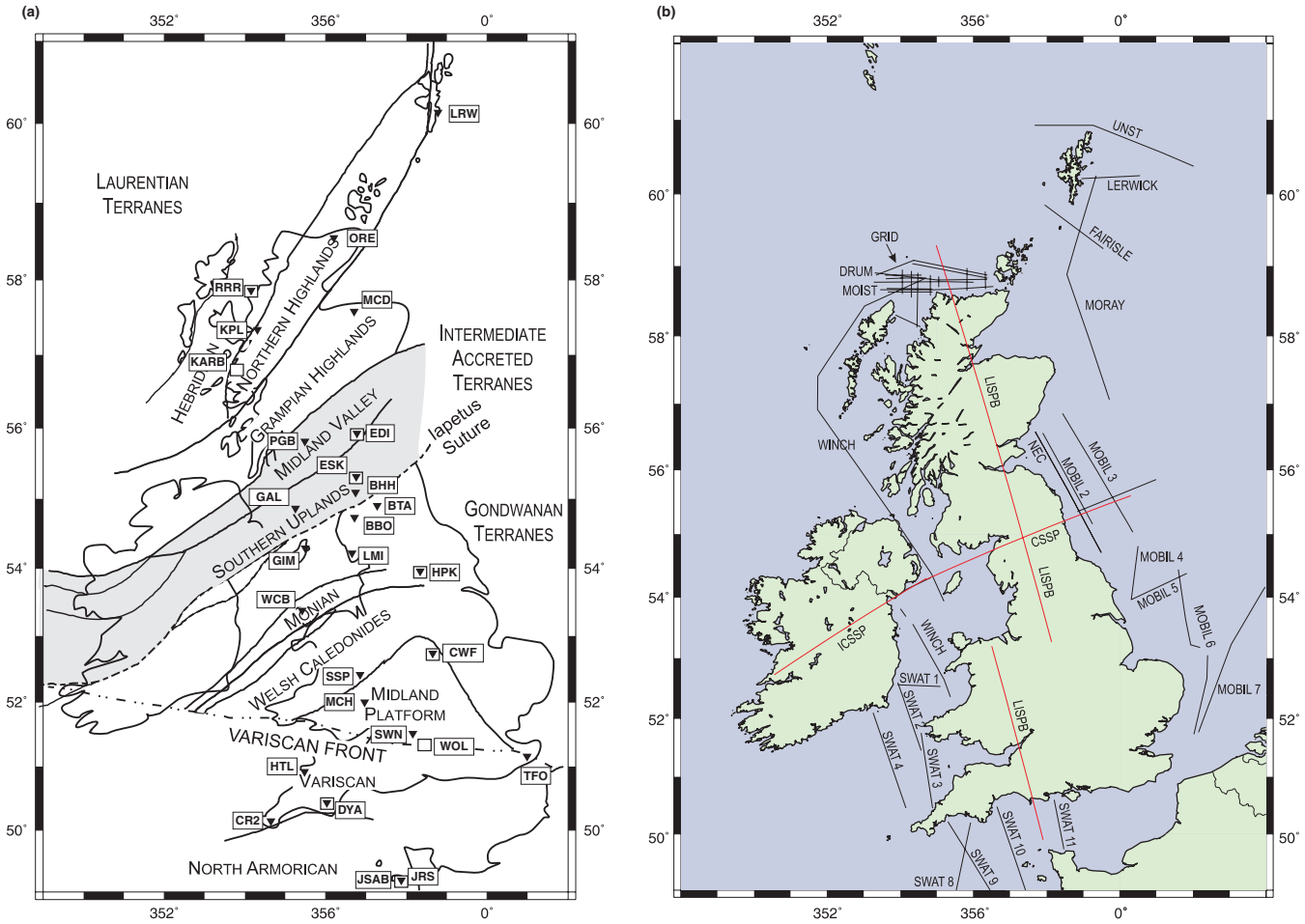

Figure 1. (a) A geological terrane map of the British Isles, after British Geological Survey (1996). The broad-band three-component instruments are marked by squares and the short-period instruments by inverted triangles. (b) A map of the deep seismic refraction and reflection profiles covering the study area.

profiles providing control on the onshore crustal and upper mantle velocity structure relevant to this study. Results from the dense coverage of offshore seismic reflection data and the limited amount of deep onshore data have been compiled into a Moho depth map (Chadwick & Pharaoh 1998) with values ranging between 25 km (northern Scotland) and 36 km (southern England). However the onshore crustal thickness is not particularly well constrained. Data collected on the wide distribution of three-component seismic stations over the British Isles contains valuable information about all of the inferred geological terranes. The analysis of receiver functions from these stations can provide estimates of the crustal thickness and V_p/V_s ratio (controlled by the mineral composition and thermal state of the crust). There are notable differences between results from deep seismic reflection and refraction profiling across the UK; for example, the seismic refraction results do not reveal any significant variations in seismic velocity over the Iapetus Suture Zone, whereas the seismic reflection results find strong dipping reflectors at the suture. Tomlinson *et al.* (2003) investigated the receiver functions in this region, comparing the observed values with the LISPB seismic refraction model of Barton (1992), demonstrating azimuthal variations in structure not identified in previous seismic results. In this paper 1-D forward velocity models of the observed receiver function data are presented and examined to develop understanding of the processes resulting in the crustal architecture of the British Isles.

2 DATA

The data used in this study have been recorded on nine broadband and 25 short-period three-component seismometers located at 28 sites throughout the British Isles (Fig. 1). The majority of the stations are short-period instruments and are part of the British Geological Survey's seismic monitoring network. Of the nine broad-band instruments, three are permanent stations maintained by the British Geological Survey (EDI), IRIS (ESK) and the Atomic Weapons Establishment (WOL). The remaining six instruments formed part of the SPICED array that was deployed for approximately 18 months between 2000 and 2001 (Kendall & Helffrich 2001).

The teleseismic records used in this study have been retrieved from various digital archives, and derived from a list of approximately 800 events of $Mb > 6.0$ occurring between 1990 and 2001, located at epicentral distances of between 30° and 100°. The majority of the events originate from around the Pacific rim, with the more proximal events coming from Asia, and along the mid-Atlantic ocean ridge.

Receiver functions have been generated from the teleseismic data following the methodology of Ammon (1991). Pre-processing of the raw data set consisted of re-sampling the data to 0.1 s, applying a Butterworth bandpass filter between 0.1 and 4 Hz, cutting the data to include no more than 30 s before and 90 s after the *P*-wave arrival, and finally tapering the ends of the cut seismograms. Fig. 2

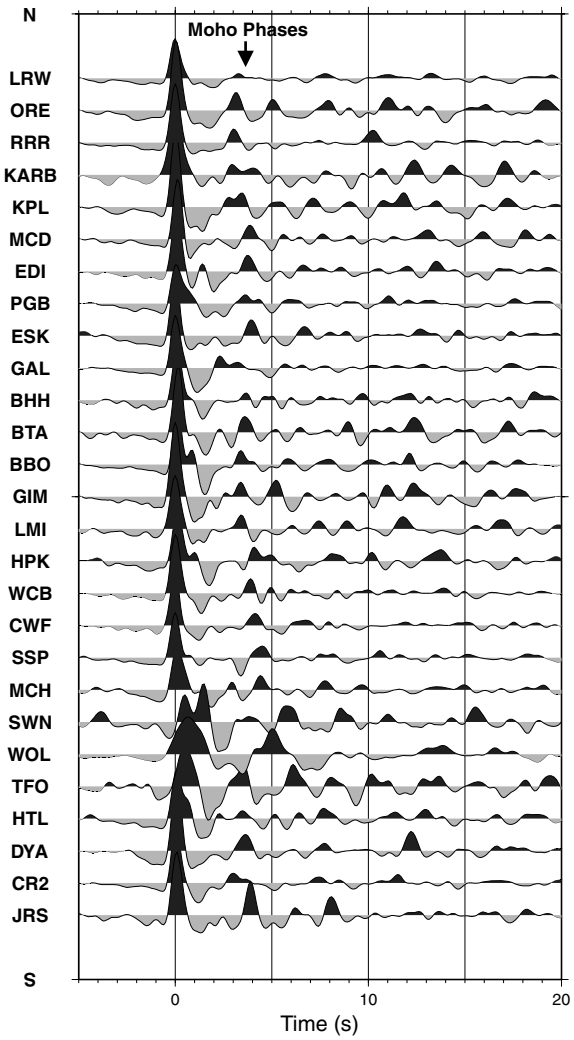

Figure 2. Stacked receiver functions from all locations, using data from all azimuths for events between 60° and 100° epicentral distance. Stacked receiver functions are plotted from north to south (see Fig. 1 for locations).

shows stacks of all of the receiver functions for each of the 28 locations. The direct *P*-wave arrivals can be seen at 0 s, the Moho *P*-to-*S* conversions (occurring at between 3 and 4.5 s) are clearly identifiable on the majority of stations.

3 $H - \kappa$ STACKING

3.1 Methodology

Multiple receiver functions can be stacked in the crustal thickness (H)–V_p/V_s ratio (κ) domain to produce a single robust estimate of H and κ (e.g. Zhu & Kanamori 2000; Cheverot & van der Hilst 2000; Ramesh *et al.* 2002). The method is applied by calculating the arrival times for the *Ps*, *PpPs* and *PsPs* (and *PpSs*) phases for a grid of $H - \kappa$ values for each receiver function of ray parameter p and average crustal *P*-wave velocity (V_p). The amplitudes of each receiver function at each of these traveltimes are summed to make the stack $S(H, \kappa)$;

$$S(H,\kappa) = \sum_{j=1\,\mathrm{to}\,n} w_1 r_j(t_1) + w_2 r_j(t_2) - w_3 r_j(t_3), \quad (1)$$

where r_j is a radial receiver function, t_1, t_2 and t_3 are the predicted *Ps*, *PpPs* and *PsPs* times, and w_1, w_2 and w_3 are weighting functions. Due to the differing moveout curves of *Ps*, *PpPs* and *PsPs* in the $H - \kappa$ domain, the point at which the phases intersect gives the unique crustal H and κ solution. This intersection point is expressed in the stack as the maximum amplitude. The primary advantages of $H - \kappa$ stacking are that; 1) the stacking is automated, rapidly producing results and negating the need to identify and pick the times of the *Ps*, *PpPs* and *PsPs* phases, and, 2) the uncertainties of the maximum point of the stack can be estimated. Zhu & Kanamori (2000) state that the Taylor expansion of $S(H, \kappa)$ at the maximum point of the stack, omitting the higher order terms, gives the variance of the stack σ in both H and κ;

$$\sigma_H^2 = 2\sigma_s \Big/ \frac{\partial^2 S}{\partial H^2}, \quad (2)$$

$$\sigma_\kappa^2 = 2\sigma_s \Big/ \frac{\partial^2 S}{\partial \kappa^2}, \quad (3)$$

where σ_s is the estimated variance of the maximum value of $S(H, \kappa)$ from the stacks of all the individual receiver functions. $\partial^2 S/\partial H^2$ and $\partial^2 S/\partial \kappa^2$ are respectively the second derivatives of the planes of constant H and κ that intersect at the maximum point of the stack. σ_H^2 and σ_κ^2 are simply a measure of the variance of the maximum point of the stack $S(H, \kappa)$ and do not include any qualitative information about the input data or any estimate of errors introduced by the choice of input Vp.

The $H - \kappa$ stacking method uses an *a priori* average crustal V_p to calculate H and κ. The primary sensitivity of the receiver function method is to velocity contrast and relative arrival times of the converted and multiple phases, and not to the absolute velocity (Ammon *et al.* 1990). The V_p/V_s ratio derived from $H - \kappa$ stacking is relatively insensitive to change in the input V_p. However, there is a considerable velocity-depth trade-off in the measurement. For earth models of a similar thickness to the crust of the British Isles there can be an approximately 1 km variation in H for a 0.2 km s^{-1} change in V_p.

3.2 Data analysis

$H - \kappa$ stacking analysis has been applied to all of the 34 broad-band and short-period three-component instruments. A total of 1493 receiver functions have been stacked for the 34 instruments. The majority of these data have been generated using a water level parameter of 0.001 and a Gaussian function $G(\omega) = e^{-\frac{\omega^2}{4a^2}}$ to limit the bandwidth of the resultant receiver function with $a = 3$ (Ammon 1991). In some cases a has been lowered to 2 to stabilize the maximum point of the stack. The trade-off in using the lower-frequency data is that the standard deviation of the maximum point of the $H - \kappa$ stack is increased. The stacking *Ps*, *PpPs* and *PpSs* times have been calculated for a range of models which increment every 0.1 km in the H domain and every 0.005 in the κ domain.

Two separate analyses have been performed on the data from the British Isles (Table 1). In Analysis 1 a constant V_p of 6.3 km s^{-1} is used to calculate the $H - \kappa$ stacks. This represents the mean *P*-wave velocity of the crust of the British Isles calculated from the principal seismic refraction studies (Barton 1992; Edwards & Blundell 1984; Jones *et al.* 1996; Al-Kindi *et al.* 2003; Grandjean *et al.* 2001). Using the fixed *P*-wave velocity allows an objective investigation of the receiver function data. In Analysis 2, where a station samples the crust close to a seismic refraction profile, the

Table 1. A table of the $H-\kappa$ stacking results for all 34 instruments from the British Isles; each stack includes n receiver functions. Listed for both analyses are V_p (km s^{-1}), crustal thickness H (km), V_p/V_s ratio κ, and their respective standard deviations defined by Zhu & Kanamori (2000) σ_H and σ_κ. Poisson's ratio σ is also presented. Analysis 1 uses a constant V_p whereas Analysis 2 uses V_p derived from local crustal seismic refraction studies. The source publication of the V_p used in Analysis 2 is listed; a = Jones *et al.* (1996), b = Barton (1992) and c = Edwards & Blundell (1984). Finally Q describes the quality of the resultant stack.

		Analysis 1						Analysis 2							
	n	V_p	H	σ_H	κ	σ_κ	σ	V_p	*Ref.*	H	σ_H	κ	σ_κ	σ	Q
LRW	52	6.30	32.8	1.88	1.66	0.10	0.215	6.30	–	32.8	1.88	1.66	0.10	0.215	2
ORE	41	6.30	26.1	1.20	1.74	0.07	0.253	6.37	*ab*	26.4	1.28	1.74	0.06	0.253	1
RRR	48	6.30	24.3	1.08	1.75	0.07	0.258	6.37	*b*	24.6	1.17	1.75	0.07	0.258	1
RRRB	28	6.30	24.2	0.94	1.76	0.07	0.264	6.37	*b*	24.6	1.04	1.76	0.07	0.262	1
MCD	59	6.30	31.2	1.45	1.76	0.07	0.262	6.24	*b*	30.7	1.46	1.76	0.06	0.264	1
KARB	11	6.30	28.3	0.84	1.83	0.06	0.289	6.37	*b*	28.7	0.92	1.82	0.06	0.285	2
KPL	67	6.30	28.0	0.96	1.75	0.06	0.256	6.37	*b*	28.3	0.98	1.75	0.06	0.256	1
EDI	73	6.30	32.6	1.39	1.71	0.07	0.238	6.54	*b*	34.0	1.58	1.70	0.07	0.235	1
EDIB	27	6.30	34.3	1.84	1.68	0.09	0.226	6.54	*b*	36.3	2.00	1.67	0.08	0.218	2
PGB	23	6.30	30.3	1.86	1.77	0.11	0.266	6.54	*b*	26.2	1.92	1.88	0.13	0.303	2
ESK	39	6.30	29.5	0.80	1.81	0.05	0.282	6.35	*b*	30.2	0.92	1.79	0.05	0.275	1
ESKB	134	6.30	30.8	1.53	1.77	0.09	0.268	6.35	*b*	31.0	1.63	1.77	0.08	0.268	1
BTA	53	6.30	29.3	1.16	1.75	0.07	0.256	6.25	*b*	29.1	1.23	1.75	0.07	0.256	1
BHH	26	6.30	27.3	1.33	1.81	0.09	0.280	6.25	*b*	27.0	1.35	1.81	0.08	0.282	1
GAL	48	6.30	31.6	2.71	1.60	0.12	0.179	6.25	*b*	29.0	2.82	1.65	0.15	0.210	2
BBO	85	6.30	28.9	0.80	1.72	0.05	0.242	6.25	*b*	28.6	0.84	1.72	0.05	0.245	1
GIM	49	6.30	29.8	1.23	1.69	0.06	0.228	6.25	*b*	29.6	1.15	1.68	0.05	0.226	1
LMI	60	6.30	27.9	1.20	1.75	0.07	0.260	6.25	*b*	27.6	1.23	1.75	0.07	0.260	1
HPK	35	6.30	32.0	1.09	1.78	0.06	0.271	6.25	*b*	31.8	1.17	1.78	0.06	0.271	1
HPKB	20	6.30	31.7	0.91	1.78	0.05	0.271	6.25	*b*	31.4	0.94	1.78	0.05	0.271	1
WCB	37	6.30	27.6	1.40	1.85	0.09	0.295	6.36	*c*	27.7	1.45	1.85	0.08	0.295	2
CWF	66	6.30	35.8	1.71	1.71	0.07	0.240	6.36	*c*	36.2	1.83	1.71	0.07	0.240	2
CWFB	25	6.30	36.1	1.66	1.71	0.07	0.240	6.36	*c*	36.5	1.74	1.71	0.07	0.240	2
MCH	42	6.30	35.3	1.99	1.77	0.08	0.268	6.36	*c*	35.9	2.00	1.76	0.07	0.264	2
SSP	60	6.30	36.0	1.67	1.75	0.09	0.256	6.36	*c*	36.4	1.80	1.75	0.08	0.256	2
SWN	31	6.30	48.8	1.48	1.72	0.05	0.245	6.24	*c*	48.3	1.43	1.72	0.05	0.245	3
WOL	53	6.30	38.9	1.99	1.79	0.07	0.273	6.24	*c*	39.0	2.03	1.78	0.06	0.269	2
TFO	18	6.30	34.1	1.84	1.61	0.08	0.186	6.30	*x*	34.1	1.84	1.61	0.08	0.186	3
HTL	42	6.30	31.5	1.37	1.66	0.08	0.212	6.30	–	31.5	1.37	1.66	0.08	0.212	2
CR2	55	6.30	28.1	0.73	1.67	0.05	0.218	6.30	–	28.1	0.73	1.67	0.05	0.218	1
DYAB	8	6.30	28.4	0.76	1.79	0.05	0.275	6.30	–	28.4	0.76	1.79	0.05	0.275	1
DYA	29	6.30	28.4	0.81	1.80	0.06	0.277	6.30	–	28.4	0.81	1.80	0.06	0.277	1
JRS	34	6.30	32.3	1.60	1.74	0.07	0.251	6.30	–	32.3	1.60	1.74	0.07	0.251	2
JSAB	15	6.30	31.3	1.04	1.76	0.05	0.264	6.30	–	31.3	1.04	1.76	0.05	0.264	1

input P-wave velocity is simply the mean crustal velocity at that point along the profile. Some of the seismic recording stations do not lie directly upon any seismic refraction profile; in this case V_p has either been left at 6.3 km s^{-1}, or if this is not an appropriate value then a regional mean velocity has been used. Examples of $H-\kappa$ stacks for the data from stations RRR, BTA, CWF and DYA are shown in Fig. 3. The amplitudes of the $H-\kappa$ stacks have been normalized relative to the amplitude at their maximum value, which defines the measured H and κ, and the plots show normalized stack contours for values above 0.6.

3.3 Error analysis

The standard deviations of the solutions estimated during the stacking procedure (Table 1) only reflect the measured standard deviation of the maximum point of the stack, and do not include any estimate of other errors that may occur; for example the use of an inappropriate stacking V_p, or departure from the 1-D approximation. This estimate does not include any qualitative information about the input receiver functions, for example as to whether the phases that produce the maximum stacking point are in fact the Moho *Ps*, *PpPs* and *PpSs*/*PsPs* phases.

3.3.1 Stack quality

In order to provide a qualitative description of the results, each $H-\kappa$ stack has been categorized as either high (1) intermediate (2) or low quality (3). Identification of the maxima of the $H-\kappa$ stacks is particularly dependent upon how well resolved is the *PpPs* phase. Applying a lower pass Gaussian filter when calculating the receiver functions has helped to stabilize those $H-\kappa$ stacks where the *PpPs* phase is poorly resolved. The $H-\kappa$ stack from BTA (Fig. 3b) has been classified as high quality (1); the *Ps* and *PpPs* phases that form the maximum point of the stack can be clearly identified in the raw receiver function data. The $H-\kappa$ stack from CWF (Fig. 3c) has been classified as an intermediate quality (2) stack. The *Ps* phase in the raw receiver functions is clearly identifiable but any *PpPs* phases are of much lower amplitude, bringing ambiguity to location of the maximum point of the $H-\kappa$ stack. The stack for SWN has been classified as low quality (3). The raw receiver

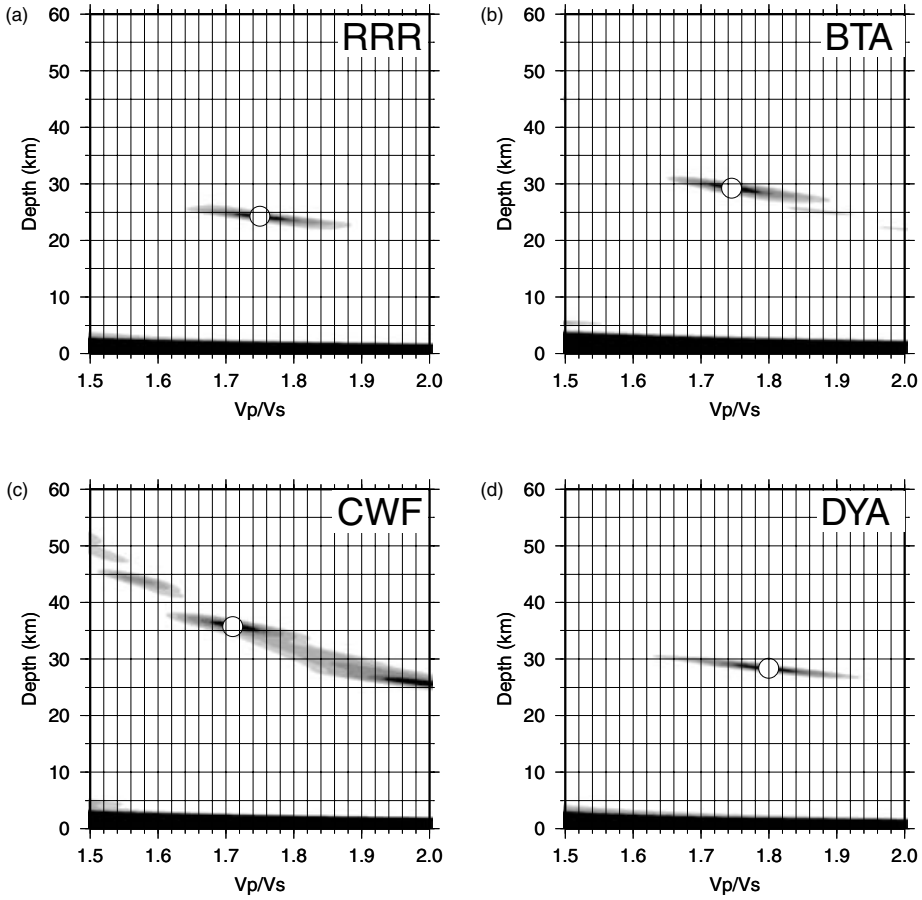

Figure 3. $H - \kappa$ stacks for stations RRR, BTA, CWF and DYA. The maximum value of each stack is marked by the open circle.

functions are dominated by many high-amplitude phases that cannot be clearly identified. This classification scheme is similar to that used by Cheverot & van der Hilst (2000) from which they provide an estimate of the quality of the $H - \kappa$ stacks from their study.

3.3.2 Velocity-depth trade-off

Constraint on the velocity-depth trade-off is provided by the LISPB onshore deep seismic refraction profile (Barton 1992; Bamford *et al.* 1978). Along the profile the average seismic velocity remains close to 6.3 ± 0.1 km s^{-1}, with the exception of the Midland Valley where it increases to >6.5 km s^{-1}. The maximum observed variation in average crustal *P*-wave velocity translates to a difference in crustal thickness estimate of between 2 to 3 km for a crust of 30 km. This is significantly smaller than the range of observed crustal thicknesses (25–35 km).

3.3.3 3-D structure

Many $H - \kappa$ stacking study authors follow Zhu & Kanamori (2000), who by stacking receiver functions from a range of different distances and directions, suppress effects of radial structure and so obtain an average 1-D crustal model beneath the recording station. To examine whether the resulting crustal thickness and V_p/V_s ratio represent the true structure beneath the station in a simple 3-D environment, a series of $H - \kappa$ stacks have been performed on synthetic receiver functions from different backazimuths using a 3-D ray-tracing program (Cassidy 1992) (Fig. 4). The results show that the $H - \kappa$ stacks of the individual 3-D receiver functions from different back-azimuths do not oscillate about the 1-D solution as might be expected (Fig. 4a). The maximum up-dip receiver functions (backazimuth $= 270^\circ$) produce a lower H and higher κ than the reference 1-D stack. The down dip receiver functions produce a slightly greater H than the reference model, while κ still remains slightly higher than the true 1-D solution. It is clear that if receiver functions from an even distribution of backazimuths were stacked, the expected 1-D solution would not be obtained through the averaging process suggested by Zhu & Kanamori (2000).

The crustal thickness within the British Isles varies between 25 and 35 km, but these changes occur over large distances (Chadwick & Pharaoh 1998). It is unlikely that Moho dips are greater than 5° beneath any of the stations from which data are analysed in this study. Below this threshold the perturbation in the $H - \kappa$ stack results is <1 km for crust with a similar velocity structure to the British Isles. This difference is of a similar magnitude to the measured standard deviations of the $H - \kappa$ stacks. The dipping structures imaged within the crust and upper mantle of the British Isles by the BIRPS profiles are not associated with large velocity discontinuities (e.g. Jones *et al.* 1996), and only result in small variation in crustal thickness by applying the 1-D approximation to the $H - \kappa$ stack calculations.

4 1-D MODELLING

The crustal velocity structure beneath the stations in this study has been investigated using detailed 1-D forward modelling of the observed radial receiver function data. Following preliminary 1-D

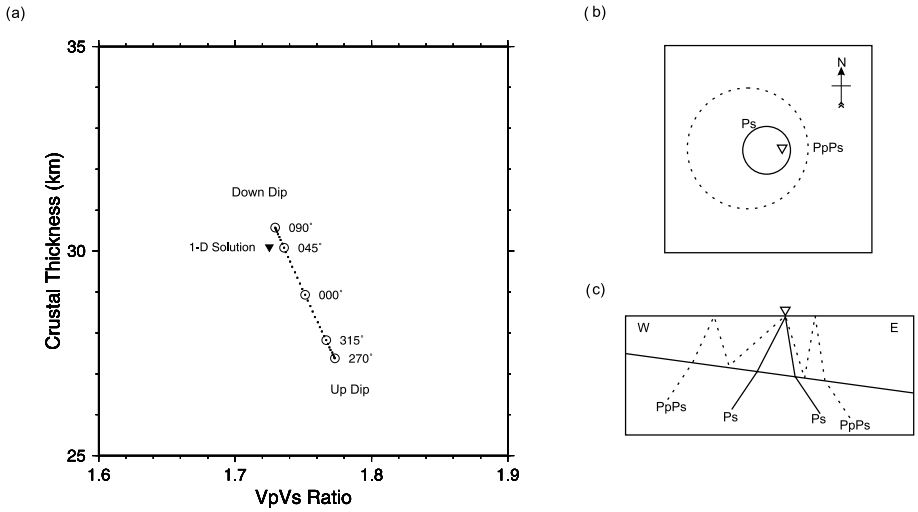

Figure 4. (a) The maximum points of $H - \kappa$ stacks for the synthetic receiver functions from a dipping Moho model. The stacks use data from variable backazimuths (labelled next to the maximum point). The 3-D model consists of a single layer crust of $H = 30$ km, $\kappa = 1.73$, $V_p = 6.3$ km s^{-1} and a Moho dipping 10° to the east. The dots are 5° increment models in between the labelled results. The inverted triangle is the $H - \kappa$ stacking result from a 1-D synthetic receiver function using identical parameters. (b) A sketch of the plan view of the lateral extent at the Moho of the *Ps* and *PpPs* phases over a dipping layer model (Cassidy 1992). (c) A sketch of the cross-sectional view of the lateral extent at the Moho of the *Ps* and *PpPs* phases through the dipping layer model.

forward results from the Iapetus Suture Zone (Tomlinson *et al.* 2003), in this study we have (1) identified the Moho *Ps* and *PpPs* phases using the results of the $H - \kappa$ stacking, and (2) fitted the remaining phases in the observed receiver functions as conversions and multiples from specific velocity discontinuities by iterative modification of simple velocity models. Receiver functions are primarily sensitive to velocity contrast and relative arrival times of phases (Ammon *et al.* 1990). To limit uncertainty introduced by the velocity-depth offset of the model it is necessary to constrain the output models with *a priori* velocity data. This modelling approach allows a good estimate of the receiver function velocity discontinuity structure to be developed, while honouring the velocity information of previous seismic studies.

The synthetic seismograms have been calculated using the method of Ammon (1991); this code is based upon the reflection matrix synthetic seismogram code of Kennett (1983). The modelling study has been carried out on stacks of the observed receiver functions. The variability of these stacked receiver functions has been estimated by calculating the standard deviation of each point in the receiver function stack. The short-period data have been modelled by limiting the bandwidth of the synthetic seismograms, reproducing the negative lobes that ring the receiver function phases, which are caused by performing the deconvolution with the limited bandwidth data. Where broad-band and short-period receivers were co-located, examination of the two data sets has shown that the resultant velocity models are comparable.

The results of receiver function modelling are non-unique. There are three crustal model parameters which control the observed and synthetic receiver functions: (1) the depth to seismic velocity interfaces, (2) the *P*-wave velocity, and (3) the *S*-wave velocity (or V_p/V_s ratio). As already noted with the $H - \kappa$ stacking analysis, there is a velocity-depth trade-off when fitting the phases of the observed receiver functions. The steps used in the 1-D forward modelling procedure, to maximize model constraint and minimize non-uniqueness, are subjective and may result in models that contain structures which are not specifically required to fit the observed data. Unconstrained linear inversions of the broad-band receiver function data have been performed to provide an estimate of the significance of the *a priori* structures which have been incorporated into the 1-D forward models. Inversions of the data from the short-period stations have not been performed to avoid mis-interpretation of the negative deconvolution ringing lobes as significant crustal velocity structures.

5 RESULTS

A summary of all of the $H - \kappa$ stacking and 1-D forward models that fit the observed receiver functions from the stations in the British Isles is presented in Figs 5(a) and (b). Only models for stations where high-quality data have been recorded are presented. Where two instruments are co-located, a representative model is presented.

The results from $H - \kappa$ stacking Analysis 1 are presented as maps of crustal thickness and V_p/V_s ratio across the British Isles (Figs 6a and b). There is considerable variation in crustal thickness over the British Isles, consistent with the seismic reflection crustal thickness variations presented by Chadwick & Pharaoh (1998), and to some extent correlating with the underlying terrane geology. The variation in V_p/V_s ratio follows a less consistent pattern than crustal thickness.

5.1 Near surface structure

Many of the 1-D models from the stations in the British Isles include significant velocity contrasts at less than 5 km depth (e.g. Figs 5 and 7d–f). Their effects on the observed receiver functions are variable. In the data from the southeast of England (SWN, WOL & TFO) where the stations are located on Mesozoic sedimentary sequences, there are many high-amplitude phases that make interpretation of the deep crustal structure difficult (Fig. 2). Where the stations are located on Devonian, Carboniferous and Permian sequences (e.g. EDI, BTA) (Fig. 7) there are strong phases in the observed receiver functions but a model for the crustal structure can still be obtained. At some stations there are strong phases between the direct *P*-wave arrival and the Moho *Ps* phase. These phases can be attributed to either (1) multiple energy from near surface structures or (2) *Ps* conversions from deeper intracrustal structures. To fit the phases as

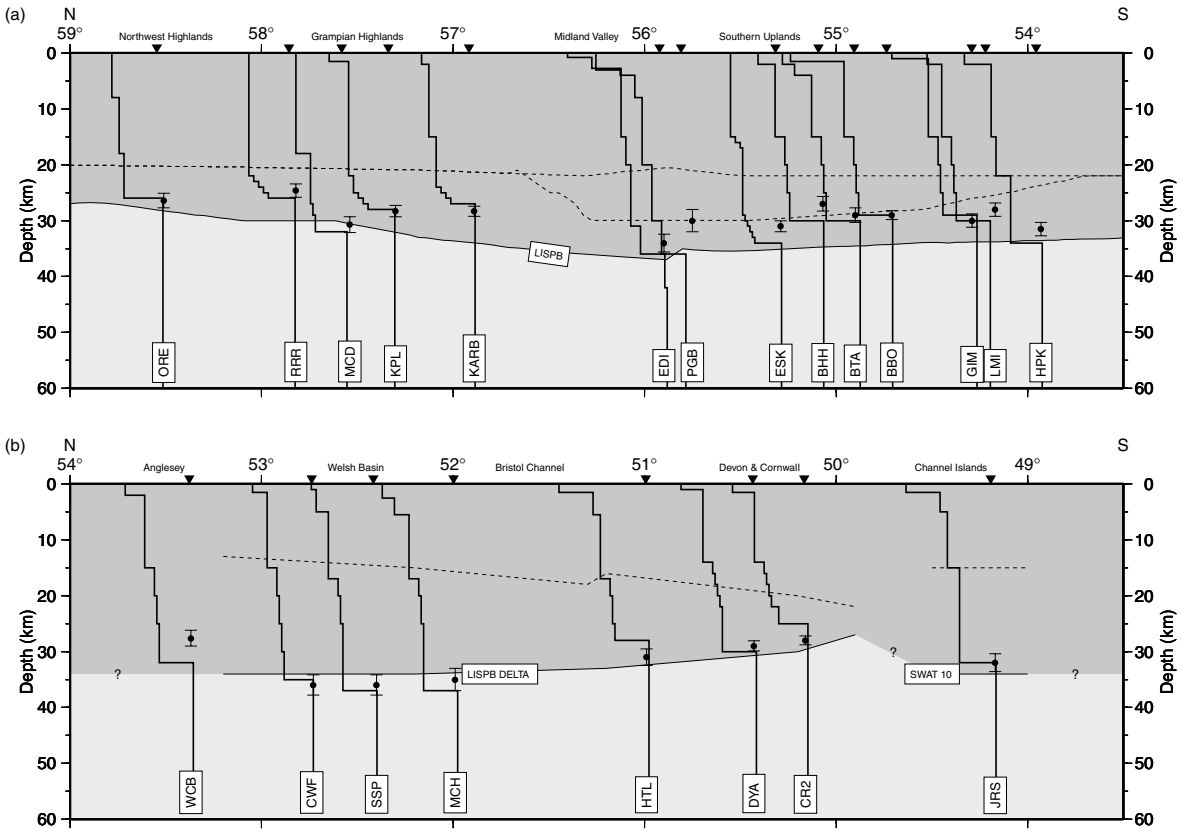

Figure 5. Results of the 1-D receiver function modelling plotted as two schematic north–south sections. The receiver function models have been plotted with the mantle layer located directly beneath the station. In section (a) the LISPB velocity model (Barton 1992) has been plotted behind the receiver function 1-D models, in (b) the LISPB Delta profile (Edwards & Blundell 1984) and SWAT10 velocity model (Grandjean *et al.* 2001) are shown. The black dots show the results of the $H - \kappa$ stacking for each station with associated $\pm 1\sigma$ error bars.

the latter requires forward models with significant velocity discontinuities in the crust. The deep seismic refraction profiles from the British Isles in general do not contain the large intracrustal velocity discontinuities required (Barton 1992; Al-Kindi *et al.* 2003), and therefore these phases have been modelled as multiples from near surface structures. The presence of near surface structure is not limited to stations that are situated on Upper Palaeozoic and Mesozoic sedimentary basins. Stations that are located on Silurian, Ordovician, Cambrian and Precambrian rocks have much lower amplitude phases from near surface structures. However, the 1-D forward models still require a velocity discontinuity in the near surface to fit the observed receiver functions. In these cases the discontinuity (generally being from $\sim$5.5 to $\sim$6.0 km s^{-1}) has been interpreted, in line with the results of seismic refraction surveys, as the contrast between Lower Palaeozoic sequences and crystalline basement rocks (e.g. Bott *et al.* 1985; Bamford *et al.* 1978; Grandjean *et al.* 2001).

5.2 Northern Scotland

The stations from Northern Scotland (LRW, ORE, MCD, RRR, KPL and KARB) sample Laurentian crust from the Hebridean, Northern Highland and Grampian Highland terranes (Fig. 1). The $H - \kappa$ stacking and 1-D forward models reveal crustal thicknesses that range between 24 and 31 km and V_p/V_s ratios that range between 1.74 and 1.76. The majority of the stations in Northern Scotland are located on Caledonian basement rocks. This is reflected in the receiver functions that are not affected by high-amplitude phases from near surface velocity discontinuities. The resultant $H - \kappa$ stacks were of high quality with the exception of those from two stations (LRW & KARB).

The stations ORE, RRR and KPL to the north and west of the region show thinner crust (24–28 km) than MCD (31 km) to the south of the Great Glen fault. The values at ORE and RRR are consistent with modelling by Asencio *et al.* (2003). The V_p/V_s ratios at these stations are similar, within the tight 1.74 to 1.76 bound. Despite the abundance of data from LRW ($n = 52$), the receiver functions show very low-amplitude *Ps* and *PpPs* conversions and this is reflected in the poorly constrained nature of the maximum point of the $H - \kappa$ stack. At KARB there are few high-quality receiver functions which may be limiting the quality of the stack. The 1-D modelling results from the stations in the northwest of Scotland show crustal thicknesses up to 3 km thinner than those beneath the LISPB profile, with MCD in the east showing slightly thicker crust. The westerly thinning of the crust is consistent with the projected crustal thinning based on the seismic reflection profiles recorded offshore west of Scotland (Chadwick & Pharaoh 1998). The receiver function data from RRR, KARB and KPL have low-amplitude *Ps* conversions from the Moho. To fit these phases a 3 to 4 km thick velocity gradient is required at the base of the crust.

5.3 Midland Valley of Scotland

The $H - \kappa$ stacks from the stations that sample the Laurentian Midland Valley of Scotland (EDI & PGB) find differing crustal

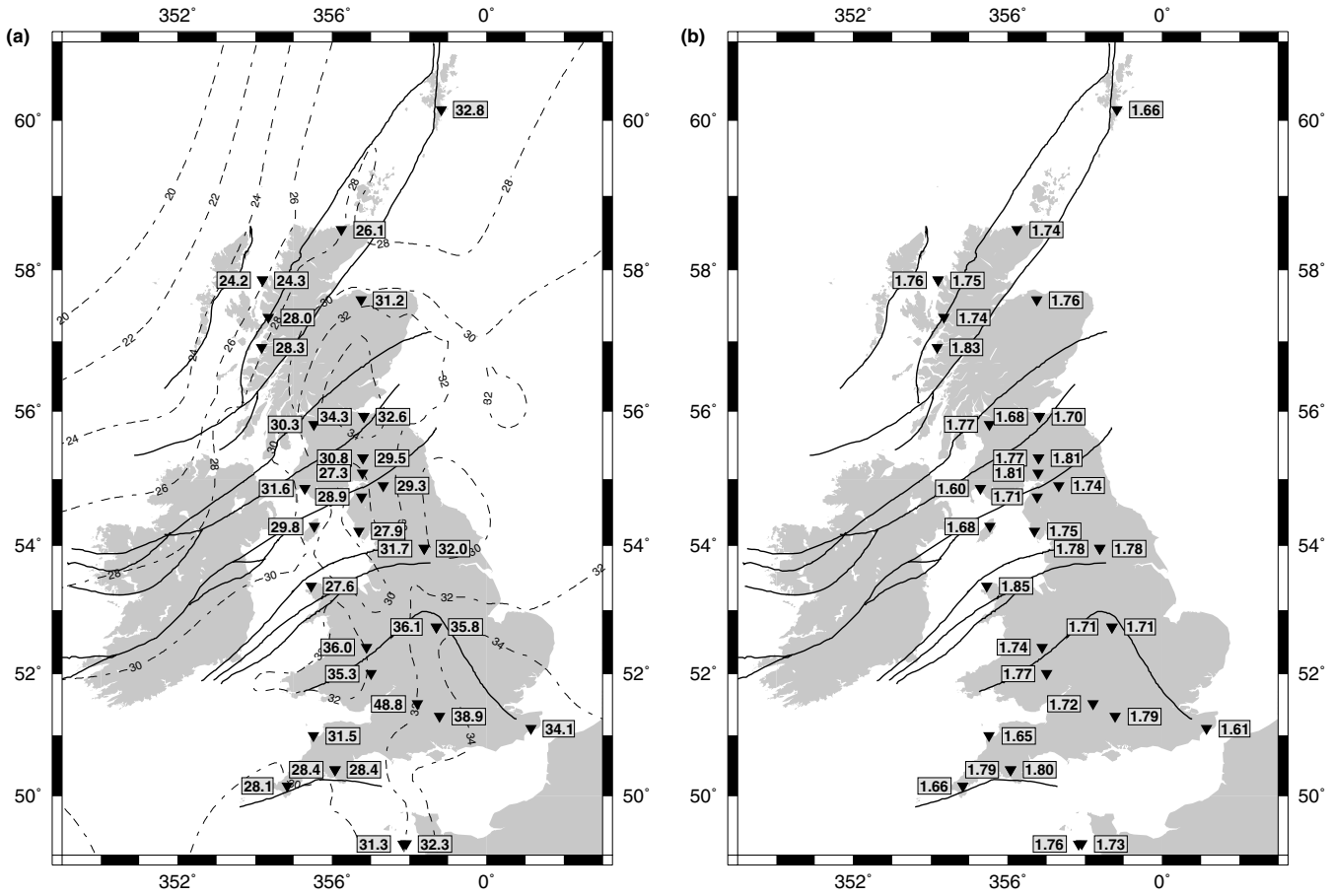

Figure 6. Maps of (a) crustal thicknesses, and (b) V_p/V_s ratio output from Analysis 1, using a constant V_p of 6.3 km s^{-1}. The crustal thicknesses reported by Chadwick & Pharaoh (1998) are contoured and plotted beneath the receiver function values. The black lines represent the terrane boundaries presented in Fig. 1.

thicknesses of 30 km in the west and 34 km in the east. The Midland Valley contains up to 5 km of Palaeozoic sediments above the Caledonian basement rocks. The velocity contrast between the sediments and the basement is seen in the 1-D forward models of the observed receiver functions (e.g. for example see Fig. 5a). 1-D forward models from both EDI and PGB show a high-velocity layer at the base of the crust, which concurs with the Barton (1992) model for the Midland Valley. The inclusion of the high-velocity layer at the base of the crust at PGB gives a crustal thickness from 1-D modelling that is 6 km thicker than the $H - \kappa$ stacking solution. The observed receiver functions for both stations have clear *Ps* phases but at PGB the *PpPs* phase is less well defined, and this may have introduced ambiguity into the $H - \kappa$ stack solution.

5.4 Iapetus Suture

The stations from the Iapetus Suture region sample the Laurentian Southern Uplands terrane to the north of the Iapetus Suture, and Gondwanan terranes to the south (ESK, GAL, BHH, BBO, BTA, GIM, LMI and HPK). The crustal thicknesses range between 27 and 31 km and the V_p/V_s ratios between 1.65 and 1.79. The near surface geology beneath the stations is variable ranging from the Ordovician–Silurian sequences of the Southern Uplands to the Carboniferous sediments of the Solway Basin. Although these near surface structures have affected the observed receiver functions and therefore the resultant 1-D models, the majority of the $H - \kappa$ stacks are of high quality (Table 1). In particular the data from ESK and BBO show very clear *Ps* and *PpPs* phases. The stack from BHH was produced using receiver function data that was calculated using the lower-frequency Gaussian filter ($a = 2$) to stabilize the initial $H - \kappa$ stack. GAL has a clear *Ps* phase but again suffers from a poorly resolved *PpPs* phase that results in a smeared maximum point of the stack.

As we have previously noted (Tomlinson *et al.* 2003), comparison between the observed receiver functions and those produced by calculating synthetic seismograms based on the LISPB model, shows that the observed *Ps* and *PpPs* phases arrive at somewhat earlier times than those predicted by the LISPB model. This time difference translates into a crustal thickness anomaly of up to 5 km between the LISPB and both the $H - \kappa$ stacking and 1-D forward receiver function models.

5.5 Central England & Wales

The stations from central England and Wales (WCB, CWF, MCH, SSP, SWN, WOL and TFO) sample the crust of the Midland Platform and Welsh basin, part of the Avalonian terrane. Station WCB lies on the suspect Monian terrane of Anglesey in North Wales. The observed receiver functions from this area contain more high-amplitude phases than are seen from elsewhere, and none of the

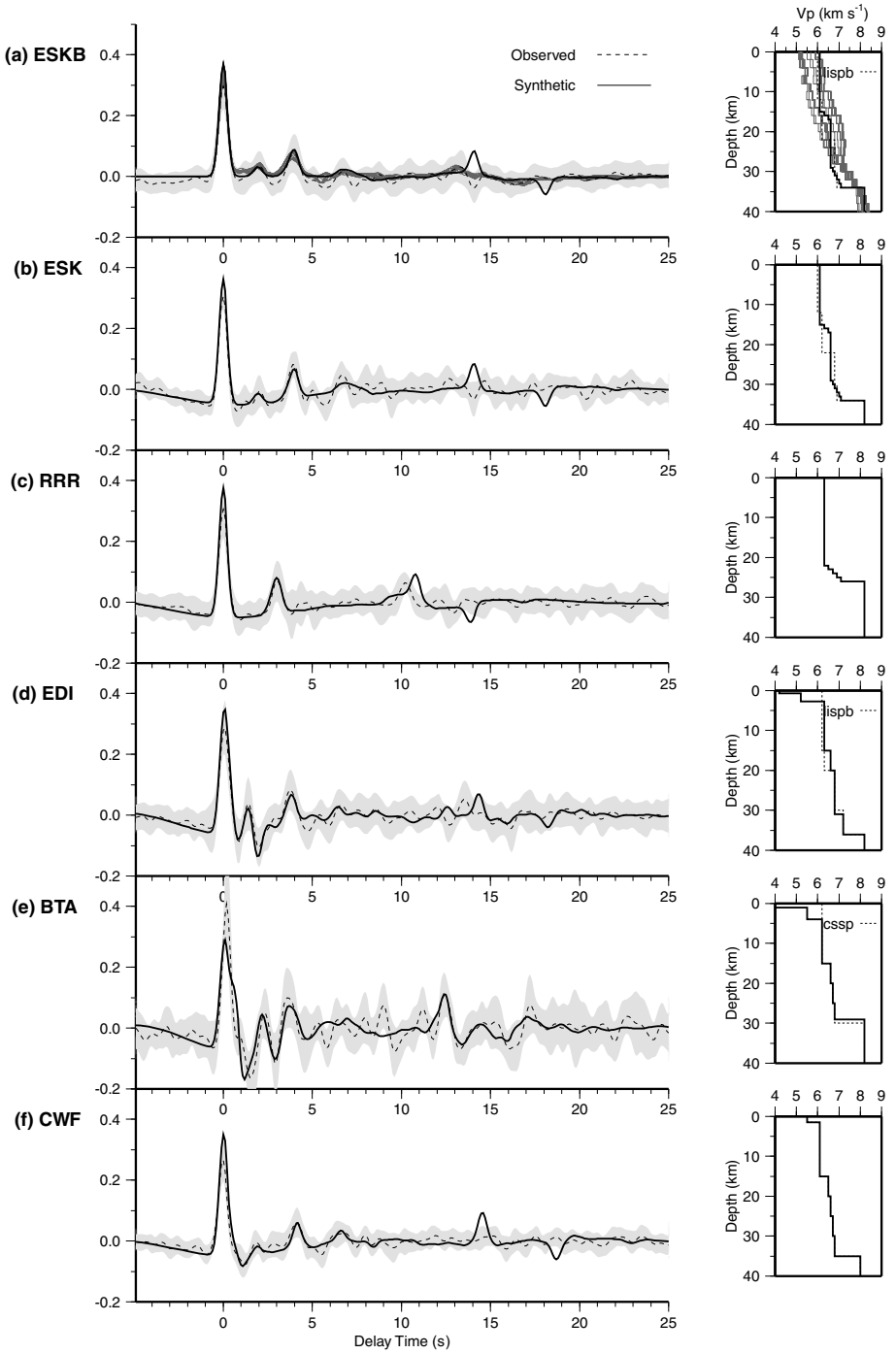

Figure 7. Examples of 1-D forward modelling results, from stations ESKB, ESK, RRR, EDI, BTA and CWF. The observed (dashed) and synthetic receiver functions are plotted, with the shading representing the standard deviations derived from the stacking of the raw receiver functions. The optimum models are shown, with the nearest seismic refraction model (dashed) where appropriate (LISPB Barton 1992; CSSP Al-Kindi *et al.* 2003). At ESKB the linear inversion models are shown (grey).

$H - \kappa$ stacks from the stations are of high quality (Table 1). Of the intermediate quality results, the crustal thicknesses are the greatest measured within the British Isles, ranging between 35 and 39 km, with the V_p/V_s ratio ranging between 1.71 and 1.79. The one exception to this is WCB which shows a much thinner 27 km thick crust and a high V_p/V_s ratio of 1.85. For the intermediate quality data the *Ps* phase is generally well defined; but the *PpPs* phases are unclear. In the case of CWF there is a high-amplitude, well-defined *Ps* phase, and a very low-amplitude *PpPs* phase.

Although there are differences in the near surface structure with stations WCB, CWF, SSP and MCH being located on Precambrian, Cambrian, Silurian and Devonian rocks, their crustal structure remains similar. Receiver function models have been derived based on

the LISPB Delta velocity model (Edwards & Blundell 1984) which incorporates two crustal layers (Fig. 5b). The boundary between the upper and lower crust has been constrained by the intracrustal *PpPs* phases at between 7 and 8s. A characteristic of the data from these stations is that the Moho *PpPs* phase is low amplitude and difficult to identify in the observed receiver functions. In some cases this has resulted in unstable $H - \kappa$ stacking. In particular it was noted that the $H - \kappa$ stacking of the data from WCB produces an unusually thin, high V_p/V_s ratio crustal model. The 1-D modelling of the data from WCB using the default V_p/V_s ratio of 1.73 reveals a crustal thickness of ∼32 km, which is much closer to the observed values at the northern end of the LISPB Delta profile (34 km) and seismic reflection data (32 km) reported by Chadwick & Pharaoh (1998).

The southern stations of SWN, TFO and WOL are located on Cretaceous sediments. The receiver functions from these stations contain many high-amplitude phases and the resultant $H - \kappa$ stacks from SWN and TFO are classified as poor quality (eq. 3). For these two stations it is possible to identify consistent phases at arrival times that correlate with Moho *Ps* phases, but there are too many high-amplitude reverberations to identify which, if any, is the Moho *PpPs* phase required to constrain the stack.

5.6 Southwest England

The few stations from the southwest of England (HTL, CR2, DYA, JRS and JSAB) are located on Avalonian crust that has been deformed by the Variscan Orogeny. For the Channel Islands stations (JRS and JSAB) the underlying crustal geology is from the Armorican terrane. The crustal thicknesses measured by those stations located on the mainland range between 28 and 31 km, and the V_p/V_s ratios between 1.66 and 1.80. The $H - \kappa$ stacks for the two stations on the Channel Islands return similar $H - \kappa$ values of ∼32 km and ∼1.75 respectively. The data from the stations in this area return high-quality $H - \kappa$ stacks with the exception of those from HTL and JRS.

The stations to the south of the Variscan front (HTL, CR2 and DYA) show a crust that at between 28 and 31 km, is 5 to 8 km thinner than the 36 km reached in central England and Wales. This thinner crust is consistent with the observations along the LISPB Delta profile (Edwards & Blundell 1984) and the seismic reflection Moho map (Chadwick & Pharaoh 1998). The V_p/V_s ratios for the stations range between 1.66 and 1.80. At HTL the near surface Carboniferous sedimentary sequences complicate the observed receiver functions, and at DYA and CR2 where the instruments are located on the Cornubian granite batholith, near surface structure is still present. Holder & Bott (1971) find that the granite extends to 10–12 km depth, so these structures must occur within the granite. In the models for HTL, DYA and CR2 there is an intracrustal structure between 14 and 17 km depth. This range is somewhat deeper than the base of the granite observed by Holder & Bott (1971), and may correlate with the R2 reflector of Brooks *et al.* (1984), which was suggested to represent a major Variscan thrust.

The stations located on the Channel Island of Jersey are the only ones from which the data sample the crust of the Armorican microcontinent. These stations show a crust that is thicker than the stations in southwest England. The two layer crust is similar to that observed at CWF, SSP and MCH located on the thick Avalonian crust. The Armorican crust, like the Avalonian crust of central England and Wales is relatively undeformed and may represent a relict fragment of a Gondwanan craton.

6 UPPER MANTLE STRUCTURE

Structures have been modelled in the uppermost mantle (<100 km depth) from the data recorded at four stations (Fig. 8).

At ORE on the northern coast of Scotland, the 'Flannan' and 'W-reflectors' (e.g. Klemperer & Hobbs 1991) have been identified in the observed receiver functions (Tomlinson *et al.* 2003; Asencio *et al.* 2003). Asencio *et al.* (2003) also identify the 'A-reflector', and suggest that their findings of multiple reflectors in the upper mantle in this region are evidence of pervasive and laterally heterogeneous velocity discontinuities related to the localized tectonic and thermal history of northwest Scotland. These results increase the plausibility of similar structures modelled within the upper mantle in this study.

Our model for the W-reflector at ORE supports the seismic refraction models of Price & Morgan (2000), showing a gradational low-velocity zone above an 8.5 km s^{-1} layer at a depth of 46 km. This, correlating with the W-reflector beneath the DRUM and GRID deep seismic refraction profiles (Klemperer & Hobbs 1991) is consistent with the reflector modelled by Asencio *et al.* (2003) at a depth of 48 km.

The data from the stations RRR, KARB (NW Scotland) and GIM (Isle of Man) have been fitted with similar models to that for ORE, indicating the presence of further subcrustal layered zones. The mantle discontinuity beneath RRR appears at 38 km, again consistent with the 39 km modelled by Asencio *et al.* (2003). At KARB, ∼100 km to the south of RRR, a similar boundary is observed at a depth of 33 km which we also suggest represents the A-reflector.

Asencio *et al.* (2003) attribute the submantle phases they have identified to thin anisotropic layers beneath these stations (∼5 km beneath RRR and ∼10 km beneath ORE) suggesting preferred orientation of olivine and orthopyroxene crystals either frozen or reoriented within a tectonic strain fabric. While these inferences are not available from our data, the indication of a deeper discontinuity beneath ORE would support the presence of there being multiple-layered reflectors in the upper mantle beneath northern Scotland.

The southward continuity of these multiple layered velocity discontinuities is unknown. However, the data from the stations in the Midland Valley contain no subcrustal structures suggesting that those in northwest Scotland must terminate or pinch out toward the south. However an equivalent structure is seen beneath GIM on the Isle of Man. Models from the other stations in the Iapetus Suture Zone, as well as the WINCH seismic reflection profile (Hall *et al.* 1984) do not show structures similar to that found beneath GIM, suggesting they are a local feature. If the subcrustal low-velocity zone at GIM is linked to subduction related metasomatism (as has been suggested for the low-velocity zone above the W-reflector (Price & Morgan 2000)), then it may represent a relic subduction zone formed during the closure of the Iapetus Ocean. While speculative, this is in accord with the suggestion of Asencio *et al.* (2003) that '. . . a complex history at the local and regional scale may play a very important role in the observed characteristics of these velocity discontinuities in the mantle lithosphere'.

7 DEPTH DEPENDENCE OF V_p/V_s

To examine the relationship between the observed crustal thicknesses and V_p/V_s ratios, the results of all of the $H - \kappa$ stacks have been plotted (Fig. 9). Plotting the data in this way can highlight clusters or trends and therefore allow classification of the crust by these populations (Cheverot & van der Hilst 2000). The plot of the results from the British Isles shows the regional crustal thickness variations already identified. However, as a complete data set the results reveal

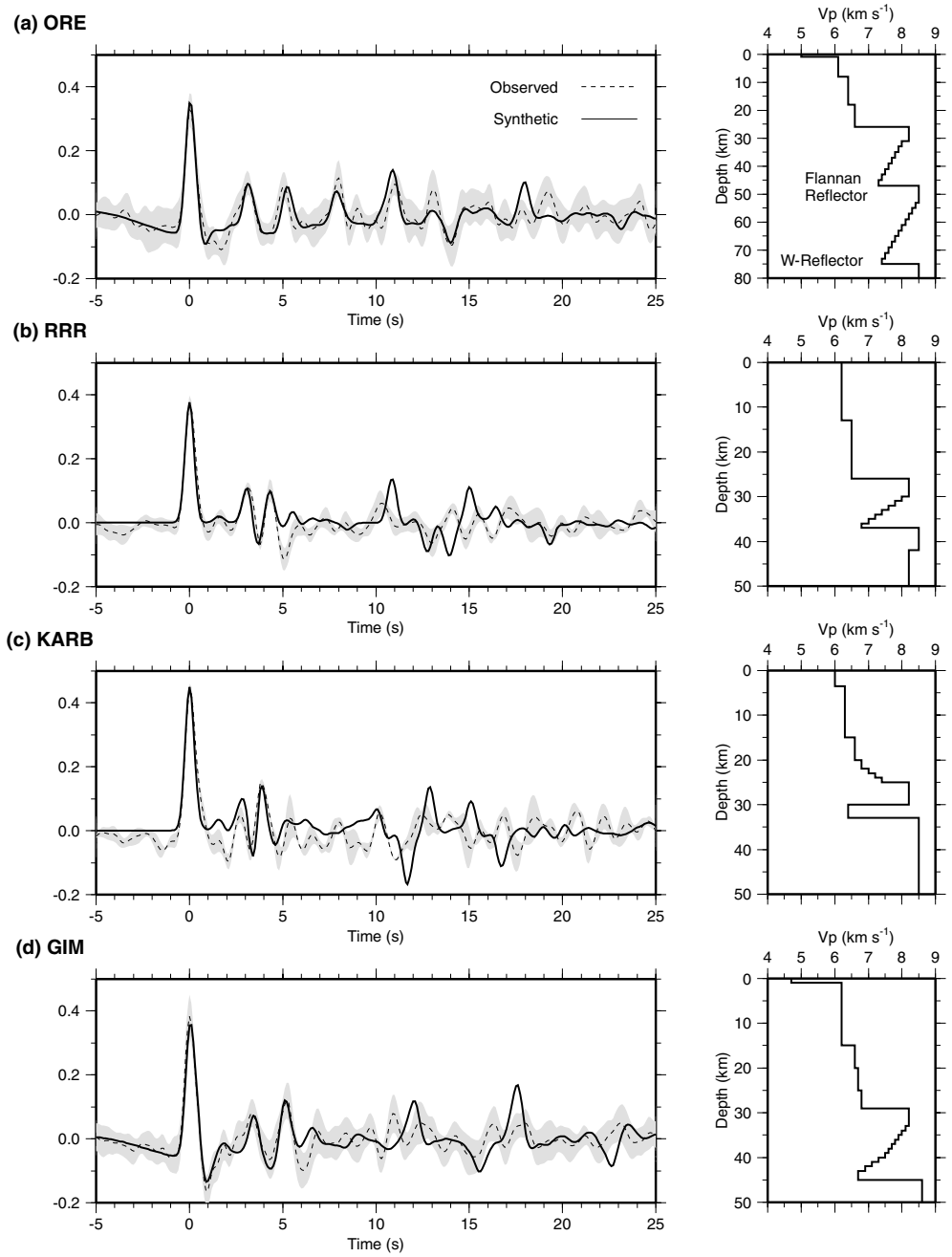

Figure 8. The 1-D receiver function models from the British Isles including upper mantle structure: (a) the receiver function data and model from ORE identifying the W and Flannan reflectors; (b) the broad-band receiver function data and model from RRR; (c) the broad-band receiver function data and model from KARB; and (d) the receiver function data and model from GIM.

no clear relationship between observed crustal thickness and V_p/V_s ratio. The stations from the north of Scotland produce the highest quality $H-\kappa$ stacks. The range of observed V_p/V_s ratios (1.74–1.76) is close to the average for extended continental crust (Christensen & Mooney 1995). This small variation in κ over crustal thicknesses between 24 and 31 km would suggest that although the thickness of the crust may be varying, the bulk crustal composition remains stable.

Results from many geophysical studies of the structure of the British Isles, including this one, suggest that there is a high-velocity layer at the base of the crust (e.g. Al-Kindi *et al.* 2003; Barton 1992). Clift & Turner (1998) studied crustal uplift across the British Isles and showed that their observations could be caused by up to 4 km of magmatic underplating at the base of the crust. If the high-velocity layer at the base of the crust does result from basic magmatic underplating, it would be reasonable to expect that the bulk crustal V_p/V_s ratio would increase (Cheverot & van der Hilst 2000). The change in bulk V_p/V_s ratio has been calculated for varying thicknesses of underplated material (Fig. 9). The example uses a continental crust of thickness = 25 km, $V_p = 6.3$ km s^{-1} and $\kappa = 1.73$ ($\sigma = 0.25$) and underplated gabbroic material of $V_p = 7.3$ km s^{-1} and $\kappa = 1.84$ ($\sigma = 0.30$). This model produces an increase in average crustal κ of

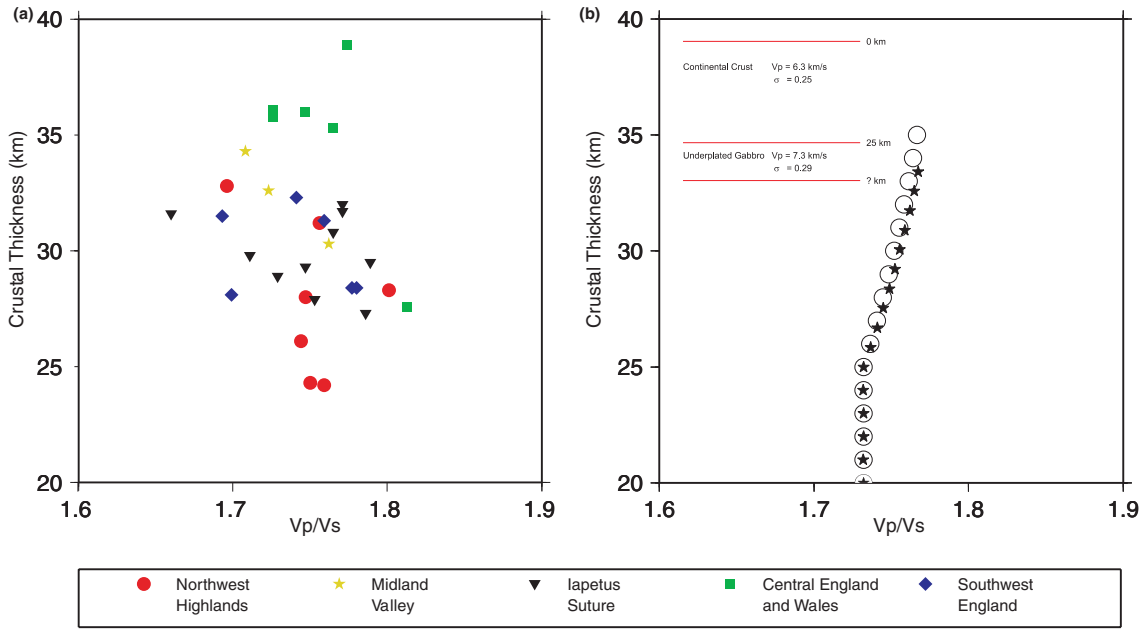

Figure 9. (a) A cross-plot of all of the $H - \kappa$ stacking values calculated using a stacking velocity of $V_p = 6.3$ km s^{-1}. The results are ornamented by geological terrane. (b) An example of the variation in V_p/V_s ratio when a layer of an increasing thickness of gabbro is added to continental crust. Circles represent the true model, stars represent the $H - \kappa$ stacking solution calculated using $V_p = 6.3$ km s^{-1}.

0.04 for a 10 km thick layer of underplate. The maximum suggested thickness of underplated material of ∼4 km suggested by Clift & Turner (1998) would only produce an increase in κ of ∼0.02. Variations of such small magnitude are below the resolution of the V_p/V_s values obtained here.

8 CRUSTAL THICKNESS ANOMALY

The results from receiver function analysis of the data from the stations in the Iapetus Suture region do not agree with the crustal thicknesses from the previous seismic refraction studies (e.g. Barton 1992; Al-Kindi *et al.* 2003). The stations to the south of the Midland Valley (ESK, BHH, BTA, BBO, GIM, LMI & WCB) which span the region directly above the Iapetus Suture Zone have crustal thicknesses (27–30 km) that are up to 7 km less than the LISPB model (34 km) (Barton 1992). Although these stations are not located directly on the LISPB profile, the near perpendicular CSSP deep seismic refraction profile shows that the crustal thickness remains between 32 and 34 km along strike of the structures investigated by the LISPB profile (Al-Kindi *et al.* 2003). There are several possible explanations for this mismatch:

(1) the average crustal velocity used in the receiver function modelling is too low, reducing the measured crustal thickness;
(2) the bulk crustal V_p/V_s ratio used in the receiver function modelling is too low;
(3) the seismic velocity of the crust is anisotropic, generating an underestimate in crustal thickness and
(4) the receiver function *Ps* phases are from a different interface to the Moho defined by seismic refraction.

Considering these points in turn:

(1, 2) *Incorrect average V_p and or bulk crustal V_p/V_s.*

It is possible to define the average crustal V_p with respect to the arrival time of the Moho *Ps* (T_{Ps}) and *PpPs* (T_{PpPs}) phases, the crustal thickness (H) and the ray parameter of the teleseismic event (p):

$$V_p = \sqrt{\frac{1}{\frac{(T_{PpPs} - T_{Ps})^2}{4H^2} + p^2}}. \quad (4)$$

By fixing the value of H and using the times of the Moho *Ps* and *PpPs* phase from the results of $H - \kappa$ stacking it is possible to test the *P*-wave velocity that is required to make the receiver function data from the Iapetus Suture area fit the crustal thickness data from the LISPB and CSSP seismic refraction experiments. To fit a crustal thickness of 33 km with the data from BTA, the average crustal *P*-wave velocity must be ∼7.1 km s^{-1}, with a V_p/V_s ratio of 1.74. To fit the same crustal thickness model with the data from BHH, V_p must increase to ∼7.5 km s^{-1}, with a V_p/V_s ratio of 1.79. These values for V_p represent a significant increase in average crustal *P*-wave velocity. Deep seismic refraction studies of the British Isles reveal the average crustal *P*-wave velocity varies between 6.2 and 6.6 km s^{-1}, and it is unlikely that an average velocity of between 7 and 7.5 km s^{-1} is reached beneath the Iapetus Suture region. Fixing the crustal thickness, H, allows a unique solution for both V_p and V_p/V_s to be calculated. These calculations show that the V_p/V_s ratios for BTA ($H - \kappa$ stacking $V_p/V_s = 1.75$) and BHH ($H - \kappa$ stacking $V_p/V_s = 1.81$) are only altered slightly relative to the $H - \kappa$ stacking results when H is fixed. This again highlights the fact that although there is a velocity-depth trade-off in the modelling of receiver function data, the calculated V_p/V_s ratio is relatively insensitive to changes in H and V_p.

(3) *Anisotropic crustal velocity.*

The ray paths of the phases used in receiver function studies are close to vertical, whereas the ray paths of phases constraining the velocities in seismic refraction studies are predominantly horizontal. If the seismic velocity of the rocks beneath the British Isles is anisotropic, then it is likely a mismatch between the receiver function and seismic refraction results may occur if the data are interpreted without considering this anisotropy. The possibility of

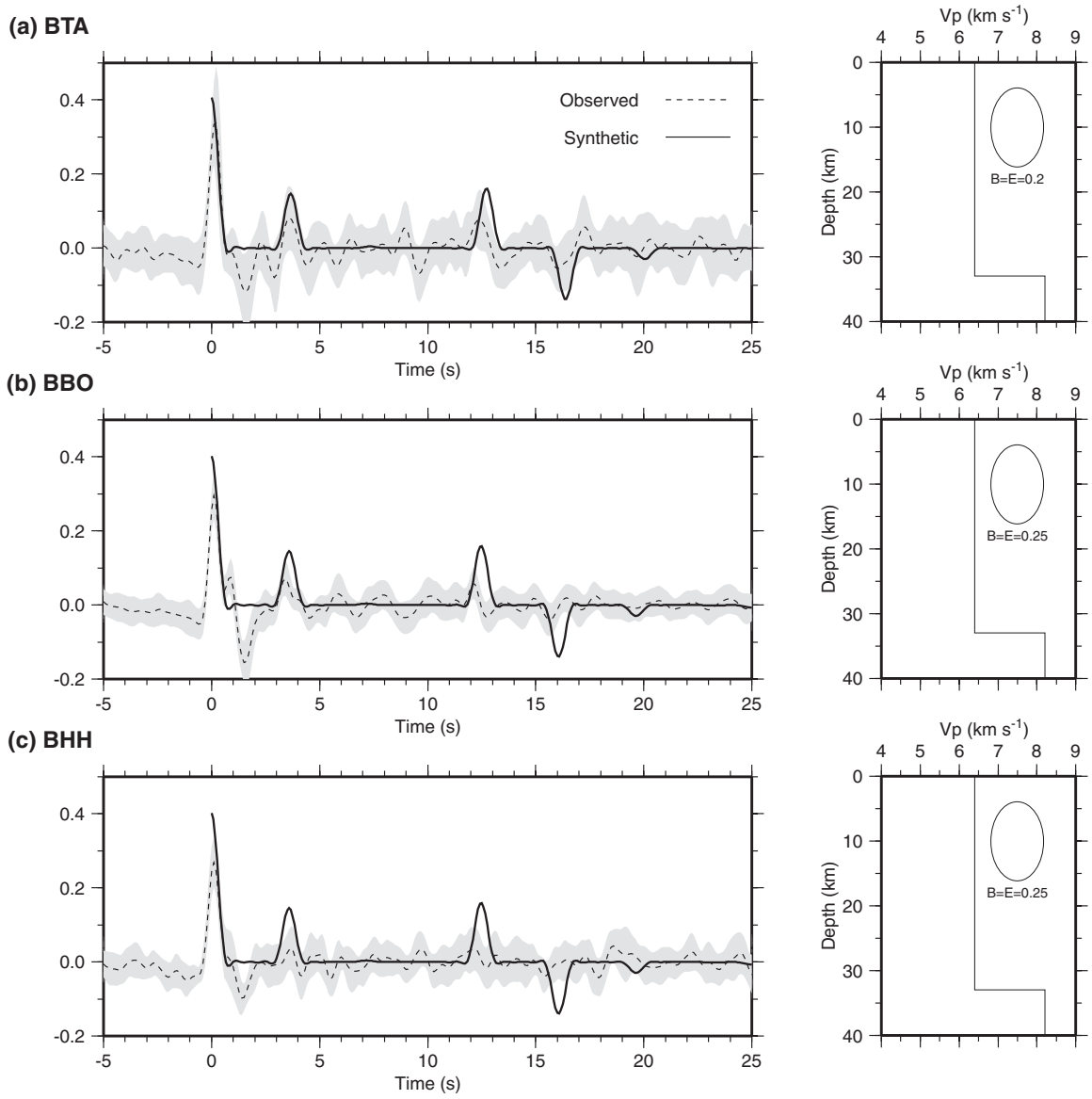

Figure 10. The results of the modelling of receiver function data from the Iapetus Suture Zone using the seismic velocity anisotropy code of Levin & Park (1998): (a) a model with the anisotropy ellipse with a vertical axis of symmetry and 20 per cent anisotropy is required to fit the timing of the phases in the observed receiver functions at BTA if the crustal thickness = 33 km and $V_p = 6.4$ km s^{-1}; (b) the data from BHH require an anisotropy model with 25 per cent anisotropy and (c) the data from BBO require an anisotropy of 25 per cent.

seismic velocity anisotropy causing the observed mismatch between the seismic refraction and receiver function models has been tested using code which incorporates anisotropy into the forward model (Levin & Park 1997, 1998). Figs 10(a)–(c) show that, if the crust close to the Iapetus Suture has a thickness of 33 km and a horizontal *P*-wave velocity of 6.4 km s^{-1} (as indicated by seismic refraction (Barton 1992; Al-Kindi *et al.* 2003)), to then fit the observed receiver functions there must be a bulk crustal *P*- and *S*-wave anisotropy of 20–25 per cent, with the fast axis of the anisotropy ellipsoid being vertical.

Seismic velocity anisotropy can be caused by several mechanisms. In the upper crust the main cause of anisotropy is thought to be the presence of aligned cracks and pore space. In the lower crust it is assumed that the cracks are closed and lattice preferred orientation of mineral crystals is the main cause of anisotropy (Levin & Park 1998). Jones *et al.* (1996) studied the mismatch between seismic reflection and seismic refraction results offshore the north of Scotland. They found that the seismic reflection Moho is deeper than the seismic refraction Moho. A bulk crustal seismic velocity anisotropy of ∼7 per cent was required to eliminate the mismatch between the two data sets, with the fast axis of the anisotropy ellipsoid being horizontal. If anisotropy is the cause of the different receiver function and seismic refraction estimates of crustal thickness then it has to be caused by a different mechanism to the anisotropy observed beneath the North of Scotland.

(4) *Conversions from an interface above the Moho.*
It seems unlikely, given the changes in bulk crustal V_p and the magnitude of the seismic velocity anisotropy required to fit the observed data for a reasonable crustal thickness of 33 km, that the observed receiver function phases are caused by the seismic refraction Moho defined by Barton (1992) and Al-Kindi *et al.* (2003). Recent results from studies of crust/upper mantle structure of the Ethiopian

rift (Mackenzie *et al.* 2005; Maguire *et al.* 2006; Stuart *et al.* 2006) show a similar mismatch in crustal thickness estimates from seismic wide-angle reflection/refraction and receiver function modelling. The latter identifies the principle base crustal receiver function *Ps* conversions near the top of a high-velocity ($V_p \sim 7.4$ km s^{-1}) underplate layer identified from the controlled source survey (Mackenzie *et al.* 2005). It is possible that the base of the underplate layer is gradational owing to the method of emplacement and, therefore, does not provide a significant receiver function conversion (Stuart *et al.* 2006).

Jones *et al.* (2002) suggest the locus of maximum Cenozoic denudation in the British Isles is centred on north England and the Irish Sea, and that the denudation is driven mainly by permanent uplift resulting from magmatic underplating, the greatest amount of melt being added to the crust beneath this region. Al-Kindi *et al.* (2003) model a welt shaped high-velocity layer in the CSSP/ICCSP data which is centred upon the uplift maximum in the middle of the Irish Sea. They conclude that this high-velocity body is underplated magmatic material, and it is this which has caused the regional uplift. The maximum thickness of this layer is ∼8 km; centred beneath the Isle of Man. The velocities within the centre of this layer are 7.2 to 7.8 km s^{-1}. The velocity of the lower crust above this layer reaches 6.6 km s^{-1}. It is likely that the phases originally considered to result from Moho conversion do in fact correspond to conversions from the top of the high-velocity layer at the base of the crust. The crustal thicknesses measured by the receiver functions correspond with the depth to the top of the high-velocity layer between ∼25 and 30 km rather than with the depth to the seismic refraction Moho at ∼33 km. The velocity model for the southern end of the LISPB profile does not include a specific layer of high-velocity underplate (Barton 1992) but does include a high-velocity layer at the base of the crust. The intersection point of LISPB and CSSP is off-centre of the maximum thickness of the underplate layer and, therefore, the presence of the underplated layer may be less obvious in the LISPB data.

The top surface of the proposed underplate defined by the receiver function models, together with the layer beneath the CSSP profile provide constraint on the minimum extent of the underplate material beneath central Britain. Fig. 11 shows that these data correspond with the area of maximum Cenozoic denudation through the East Irish Sea and northern England, as described by Jones *et al.* (2002).

The correlation of the anomalous seismic models to the denudation data support the Jones *et al.* (2002) contention that the observed uplift is caused by material from the Iceland plume, transported in a subvertical asthenospheric sheet beneath the present Faroes–Irish Sea–Lundy axis, underplating the crust. Clift & Turner (1998) suggest that the maximum thickness of underplate (>5 km) in the British Isles is beneath northwestern Scotland, corresponding with the Tertiary igneous centres of the Inner Isles. The receiver function models from this region (RRR, KPL & KARB) include a velocity gradient at the base of the crust. It may be the case that these velocity gradients represent a layer of underplate that contrasts less strongly with the overlying crustal material than that in Central Britain. The top of the gradational layers are some 3–4 km shallower than the seismic reflection Moho defined by Chadwick & Pharaoh (1998). The thickness of these gradational layers have been used to constrain the contours in Fig. 11. The receiver function models from northeastern Scotland (ORE & MCD) do not show any signs of underplated material and are consistent with the denudation observed by Jones *et al.* (2002). The receiver function results from Southern England and Wales do not indicate the presence of significant underplated material.

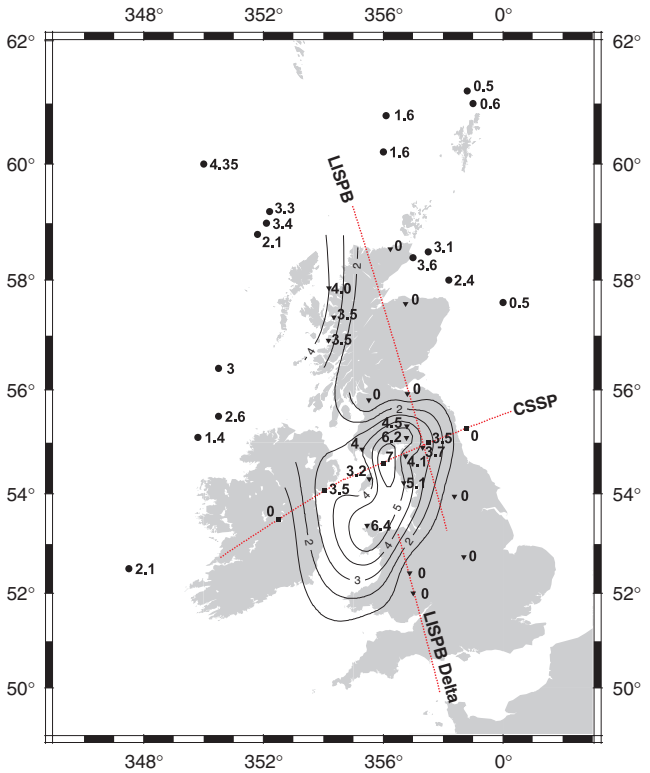

Figure 11. A map of proposed underplate thickness beneath the British Isles. The contours are derived from the underplate thicknesses interpreted from receiver function modelling (inverted triangles) and the seismic refraction velocity model of Al-Kindi *et al.* (2003) (squares). The uplift based underplate thicknesses from Clift & Turner (1998) are shown for comparison (circles). The map highlights the anomalously thick underplate layer beneath the Irish Sea and surrounding areas.

9 CONCLUSIONS

Teleseismic data from 34 broad-band and short-period instruments deployed throughout the British Isles have been investigated using receiver function analysis. $H - \kappa$ stacking has been used to produce a series of point values for crustal thickness and average crustal V_p/V_s ratio. The 1-D forward modelling of the receiver function phases has provided detailed information about the velocity-depth structure beneath each of the seismic monitoring stations.

Crustal thicknesses beneath the British Isles vary between 24 and 36 km, and V_p/V_s ratios vary between 1.60 and 1.85. In general, the models from $H - \kappa$ stacking and 1-D forward modelling correlate with the observations from previous deep seismic reflection and refraction profiles. The common features of crustal morphology that have been seen are

(1) thinning of the crust to ∼25 km in northwest Scotland,
(2) a 36 km thick crust in the Midland Valley of Scotland,
(3) a ∼36 km thick crust through central England and Wales and
(4) thinner crust (∼28 km) in the southwest of England.

The main exception to the correlation in crustal thickness identified between the receiver function models and those from previous seismic refraction studies occurs in the region surrounding the Irish Sea, where the base of the crust derived from receiver function modelling is up to 7 km shallower than the seismic refraction Moho. The source of these discrepancies was investigated, with the most likely cause being that the modelled receiver function Moho and

the seismic refraction Moho close to the Iapetus Suture are in fact different boundaries. Correlating this observation with the results of Al-Kindi *et al.* (2003) suggests that the strongest receiver function *Ps* phases from this area have originated from the top of a layer of high-velocity underplated material which is up to 7 km thick at the base of the crust. The correlation between the top of this underplate layer and the observed pattern of Cenozoic denudation over the British Isles is good, supporting the hypothesis that the underplate material was sourced from the Iceland plume.

The models from the lithospheric mantle have been compared with previous results from Asencio *et al.* (2003). We have modelled equivalent discontinuities within the lithospheric mantle beneath northern Scotland, which have been correlated with the Flannan, W- and A-reflectors identified by the BIRPS offshore reflection profiles (e.g. Klemperer & Hobbs 1991). The data from this study show that these structures must be truncated or pinch out southwards as they are not present in the receiver function data from stations in the Midland Valley of Scotland and further south. The isolated subcrustal velocity structure at GIM is similar to that found at ORE which correlates with the W-reflector. The W-reflector has been proposed as subducted oceanic crust (Price & Morgan 2000), and as such, the discontinuity found at GIM may represent a relict subduction structure resulting from the closure of the Iapetus Ocean.

ACKNOWLEDGMENTS

The work of JPT was supported by a CASE studentship at the British Geological Survey and AWE Contract OCG0385, and it is published with the permission of the Executive Director, BGS (NERC).

REFERENCES

Al-Kindi, S., White, N., Sinha, M., England, R. & Tiley, R., 2003. Crustal trace of a hot convective sheet, *Geology,* **31,** 193–288.

Ammon, C.J., 1991. The isolation of receiver effects from teleseismic P-waveforms, *Bull. seism. Soc. Am.,* **81**(6), 2504–2510.

Ammon, C.J., Randall, G.E. & Zandt, G., 1990. On the nonuniqueness of receiver function inversions, *J. geophys. Res.,* **95**(B10), 15 303–15 318.

Asencio, E., Knapp, J., Owens, T. & Helffrich, G., 2003. Mapping fine scale heterogeneities within the continental mantle lithosphere beneath Scotland; combining active and passive source seismology, *Geology,* **31**(6), 477–480.

Bamford, D., Nunn, K., Prodehl, C. & Jacob, B., 1978. LISPB — IV. Crustal Structure of Northern Britain, *Geophys. J. R. astr. Soc.,* **54,** 43–60.

Barton, P.J., 1992. LISPB revisited: a new look under the Caledonides of northern Britain, *Geophys. J. Int.,* **110,** 371–391.

Bott, M.H.P., Long, R.E., Green, A.S.P., Lewis, A.H.J., Sinha, M.C. & Stevenson, D.L., 1985. Crustal structure south of the Iapetus suture beneath northern England, *Nature,* **314,** 724–727.

Brewer, J.A., Matthews, D.H., Warner, M.R., Hall, J., Smythe, D. & Whittington, R.J., 1983. BIRPS deep seismic reflection studies of the British Caledonides, *Nature,* **305,** 206–209.

Brooks, M., Doody, J.J. & Al-Rawi, F.R.J., 1984. Major crustal reflectors beneath SW England, *J. geol. Soc. Lon.,* **141,** 97–103.

Cassidy, J.F., 1992. Numerical experiments in broadband receiver function analysis, *Bull. seism. Soc. Am.,* **82**(3), 1453–1474.

Chadwick, R.A. & Pharaoh, T.C., 1998. The seismic reflection Moho beneath the United Kingdom and adjacent areas, *Tectonophysics,* **299,** 255–279.

Cheverot, S. & van der Hilst, R.D., 2000. The Poisson's ratio of the Australian crust: geological and geophysical implications, *Earth planet. Sci. Lett.,* **183,** 121–132.

Christensen, N.I. & Mooney, W.D., 1995. Seismic velocity structure and composition of the continental crust: a global view, *J. geophys. Res.,* **100**(B7), 9761–9788.

Clift, D. & Turner, J., 1998. Paleogene igneous underplating and subsidence anomalies in the Rockall-Faeroe-Shetland area, *Mar. Petrol. Geol.,* **15,** 223–243.

Edwards, J.W.F. & Blundell, D.J., 1984. Summary of seismic refraction experiments in the English Channel, Celtic Sea and St George's Channel, Marine Geophysics Report 144, British Geological Survey.

Freeman, B., Klemperer, S.L. & Hobbs, R.W., 1988. The deep structure of northern England and the Iapetus Suture zone from BIRPS deep seismic reflection profiles, *J. geol. Soc. Lon.,* **145,** 727–740.

Grandjean, G., Guennoc, P., Recq, M. & Andréo, P., 2001. Refraction/wide-angle reflection investigation of the Cadomian crust between northern Brittany and the Channel Islands, *Tectonophysics,* **331,** 45–64.

Hall, J., Brewer, J.A., Matthews, D.R. & Warner, M.R., 1984. Crustal structure across the Caledonides from the "WINCH" seismic reflection profile: influences on the evolution of the Midland Valley of Scotland, *Trans. R. Soc. Edin. Earth Sci.,* **75,** 97–109.

Holder, A.P. & Bott, M.H.P., 1971. The crustal structure in the vicinity of south-west England, *Geophys. J. R. astr. Soc.,* **23,** 465–489.

Jones, K.A., Warner, M.R., Morgan, R.P.L., Morgan, J.V., Barton, P.J. & Price, C.E., 1996. Coincident normal-incidence and wide-angle reflections from the Moho: evidence for crustal seismic anisotropy, *Tectonophysics,* **264,** 205–217.

Jones, S.M., White, N., Clarke, B.J., Rowley, E. & Gallagher, K., 2002. Present and Past influence of the Iceland Plume on sedimentation, in *Exhumation of the North Atlantic margin*, pp. 13–25, eds Dore, A.G., Cartwright, J.A., Stoker, M.S., Turner, J.P. & White, N., Geological Society Special Publication 196.

Kendall, J.M. & Helffrich, G., 2001. Broadband Seismology SPICeD: imaging the deep Earth, *Astronomy and Geophysics,* **42**(3), 26.

Kennett, B.L.N., 1983. *Seismic Wave Propagation in Stratified Media*, Cambridge University Press, Cambridge.

Klemperer, S. & Hobbs, R., 1991. *The BIRPS Atlas: Deep Seismic Reflection Profiles Around the British Isles*, Cambridge University Press, Cambridge.

Levin, V. & Park, J., 1997. *P*-to-*SH* conversions in a flat-layered medium with anisotropy of arbitrary orientation, *Geophys. J. Int.,* **131,** 253–266.

Levin, V. & Park, J., 1998. *P*-to-*SH* conversions in layered media with hexagonally symmetric anisotropy: a cook book, *Pure appl. Geophys.,* **151,** 669–697.

Mackenzie, G.D., Thybo, H. & Maguire, P.K.H., 2005. Crustal velocity structure across the Main Ethiopian Rift: results from 2-dimensional wide-angle seismic modelling, *Geophys. J. Int.,* **162,** 994–1006.

Maguire, P.K.H. *et al*., 2006. Crustal structure of the Northern Main Ethiopian Rift from the EAGLE controlled source survey; a snapshot of incipient lithospheric break-up, in *The Afar volcanic province within the East African Rift System*, pp. 269–292, eds Yirgu, G., Ebinger, C. & Maguire, P.K.H., Geological Society Special Publication 259.

McGeary, S., Cheadle, M.J. & Blundell, D.J., 1987. Crustal structure of the continental shelf around Britain derived from BIRPS deep seismic profiling, in *Petroleum Geology of North West Europe*, pp. 33–41, eds Brooks, J. & Glennie, K.

Price, C. & Morgan, J., 2000. Lithospheric structure north of Scotland-II. Poisson's ratios and waveform modelling, *Geophys. J. Int.,* **142,** 737–754.

Ramesh, D.S., Kind, R. & Yuan, X., 2002. Receiver function analysis of the North American crust and upper mantle, *Geophys. J. Int.,* **150,** 91–108.

Stuart, G.W., Bastow, I.D. & Ebinger, C.J., 2006. Crustal structure of the northern Ethiopian Rift from receiver function studies, in *Structure and evolution of the East African Rift System in the Afar volcanic province*, eds Yirgu, G., Ebinger, C.J. & Maguire, P.K.H., Geological Society Special Publication.

Tomlinson, J., Denton, P., Maguire, P. & Evans, J., 2003. UK crustal structure close to the Iapetus Suture: a receiver function perspective, *Geophys. J. Int.,* **154,** 659–665.

Zhu, L. & Kanamori, H., 2000. Moho depth variation in southern California from teleseismic receiver functions, *J. geophys. Res.,* **105**(B2), 2969–2980.